Optical Review (2019) 26:231–240
https://doi.org/10.1007/s10043-019-00493-8

REGULAR PAPER

Dynamic Mach–Zehnder interferometer based on a Michelson configuration and a cube beam splitter system

A. Montes Pérez[1] · G. Rodríguez-Zurita[1] · V. H. Flores-Muñoz[3] · G. Parra-Escamilla[4] · D. I. Serrano-García[4] · A. Martínez-García[5] · J. M. Islas-Islas[2] · J. G. Ortega-Mendoza[6] · L. García Lechuga[2] · Noel-Ivan Toto-Arellano[2]

Received: 16 June 2018 / Accepted: 1 October 2018 / Published online: 10 February 2019

Abstract
We developed simultaneous phase-shifting system based on a Mach–Zehnder interferometer and a replicating system integrated by a Michelson configuration and a cube beam splitter. The system is capable to obtain four simultaneous interferograms in a single capture, and the phase shifts are controlled by placing a linear polarizer in each replica obtained. The system retrieves four interferograms with a relative phase shift of $\pi/2$ and the optical phase map is calculated using the four-step algorithm. In addition, the configuration presents potential capabilities for generating spiral interference patterns. To show the advantage of the technique, experimental results are presented for static and dynamic samples.

Keywords Interferometry · Phase shift · Optical metrology

1 Introduction

The development of phase-shifting interferometry (PSI) started in the decade of the 1960s with the research developed by Carré and Crate [1, 2]; later, Bruning, Wyant, Hardy, and Moore implemented these techniques for digital wavefront measuring, fringe scanning interferometry, and real-time phase correction of optical imaging systems [3–6]. Conventionally, the PSI technique generates phase shifts by stages, that is, n images are obtained in n captures of the camera. By means of the generated interferograms, the optical phase can be calculated to be associated later with the physical parameters of the sample under study.

However, the occurrence of vibrations or temporal vibrations limits the measurement system in the sequential capture. Currently, PSI techniques have been developed allowing the study of static [7–9] and dynamic events by employing polarization techniques and precision optics such as pixelated masks and holographic or diffractive elements. Using these components coupled to detection systems like cameras, or 4-f systems to the main interferometer [10–16], these systems allow the capture of several interferograms simultaneously retrieving optical phase variation instantaneously [15–23]. In the previous reports, several coupled interferometric systems have been used for the generation of simultaneous patterns; however, some of them are only capable of obtaining the phase derivative and, due to their

Electronic supplementary material The online version of this article (https://doi.org/10.1007/s10043-019-00493-8) contains supplementary material, which is available to authorized users.

✉ A. Montes Pérez
arelimp@fcfm.buap.mx

✉ Noel-Ivan Toto-Arellano
ivantotoarellano@hotmail.com;
noel.toto@utectulancingo.edu.mx

[1] Laboratorio de Óptica Física de la Benemérita, Universidad Autónoma de Puebla, 72592 Puebla, Pue, Mexico

[2] Cuerpo Académico de Ingeniería Ciencias e Innovación Tecnológica, Centro de Tecnologías Ópticas y Fotónicas, Universidad Tecnológica de Tulancingo, 43642 Tulancingo, Hidalgo, Mexico

[3] Departamento de Ingeniería Robótica, Universidad Politécnica del Bicentenario, 36283 Silao, Gto, Mexico

[4] Centro Universitario de Ciencias Exactas e Ingenierías, Universidad de Guadalajara, 44430 Guadalajara, Mexico

[5] Centro de Investigaciones en Óptica A.C, 37150 León, Gto, Mexico

[6] División de Ingenierías, Universidad Politécnica de Tulancingo, 43629 Tulancingo, Hidalgo, Mexico

base interferometer, they only have out-of-plane sensitivity. In these cases, the alignment procedures are limited for the paraxial range of the images [11–23].

For these reasons, the implementation of a simultaneous phase-shifting technique is proposed.

Our proposal is composed by the combinations of three systems: a polarizer Mach–Zehnder interferometer (MZI), which allows generating two beams at its output with orthogonally linearly polarization states; a Michelson interferometer (MI), which generates two replicas at its output, and a replication system composed by a beam splitter and mirror. As a result, eight beams are generated at its output and by alignment procedures, four interference patterns coming from the MZI are obtained and captured simultaneously. Our purpose is the development of phase dynamic interferometric configurations capable to analyze phase variation in time. Since we are not employing a micropolarizing array or diffractive elements to retrieve the necessary interferogram replicas to achieve the measurements, the system uses polarization as a phase-shifting technique on each of the replicas by controlling a polarizer [23–29].

For this configuration, the environment's vibrations mainly affect the interference generated by the Mach–Zehnder interferometer. In the case that the vibration occurs on the replication system, the interference pattern registration will be affected and re-alignment procedures need to be done. Due to the use of a cubic beam splitter and a mirror, the four images are aligned with the optical axis, so there is no need to make corrections to compensate for distortions that could be produced in the images. To show the novelty and usage of the developed system, we present the experimental results for static and dynamic variations of several phase objects.

2 Experimental setup

The diagram of the experimental setup is shown in Fig. 1. A 635 nm laser with 30 mW output is used as light source. A spatial filter system (SFS) and a collimating lens L_0 generate a plane wave front that passes through a linear polarizer (P_{45}) with fast axis orientation at 45°. The output of the MZI generates two beams with orthogonal linear polarization states. After the output of the MZI, two replication systems are used: (1) a Michelson configuration composed by a beam splitter and mirrors [M_3, M_4] (Fig. 1—MI) and (2) a beam splitter system (BSS) composed by a beam splitter (Fig. 1—BSS). Mirrors M_3–M_5 are aligned according to each obtained replica. The alignment will depend on the use; it can be a conventional interferometer or a double-window configuration. For the capture of the interferograms, a CMOS camera with an imaging lens (L_1) is used. The MZI can control the

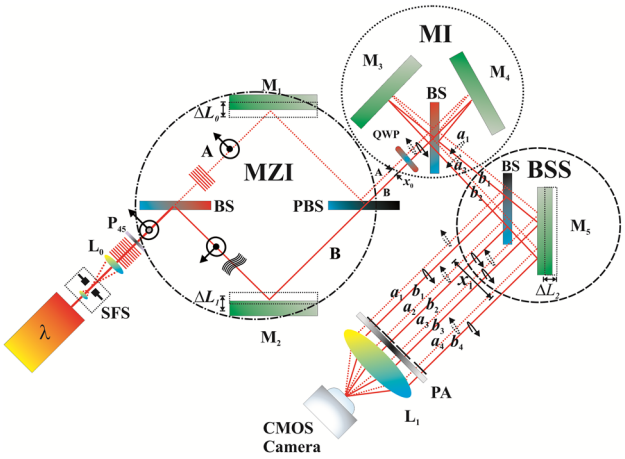

Fig. 1 Diagram of the experimental setup. Light source coming from a laser is spatially filtered and expanded by the spatial filter system (SFS) and collimating lens (L_0). Two beams are generated with the MZI with a controllable lateral separation (x_0) and replicated with the MI and BSS systems. In the figure, $M_{1,2,3,4,5}$: mirrors. *QWP* quarter wave plate, *PBS* polarizing beam splitter, *BS* beam splitter, A: reference beam. B: sample Beam. a_i,b_i: beams replicated. PA: polarizer array. L_1: imaging lens. x_0: lateral beam separation and x_1: beam separation. ΔL_i: mirror´s displacement

beam separation x_0 by controlling the displacement of mirrors M_1 and M_2.

By this property, two configurations can be obtained depending on the beam separation and beam diameter a. When the beam displacement is greater than the beam size, $x_0 > a$, the MZI operates as a double-window interferometer, by generating eight beams at the output of the complete system, as shown in Fig. 2. Figure 2a shows the two emerging beams of the MZI and Fig. 2b shows the four replicas generated after passing through the MI. In this configuration, it is necessary to replace the QWP at the output of the MZI for two QWP to cover the beams into the output of the MZI. In Fig. 2a, the QWP placed on the replicas of the beams are shown, and the continuous rectangle represents the QWP at 45° and the dotted rectangle at the QWP at 135° with respect to the polarization axis of each beam. Each QWP covers their respective patterns, and so, when they overlap, they have parallel circular polarizations, as shown in Fig. 2c. In the figure, the arrows indicate the states of polarization of the beams. In the final stage, to create the interference patterns, the superposition of the beams must be generated by moving the mirrors M_3–M_5, and this is shown in Fig. 2d. The sample must be placed in the input system, and it will operate as a shearing interferometer. One of the advantages of this configuration is that it is stable against external or environmental vibrations, and no pneumatic suspension is required to suppress vibrations [24]. However, because of the polarization states which are parallel, the range of phase

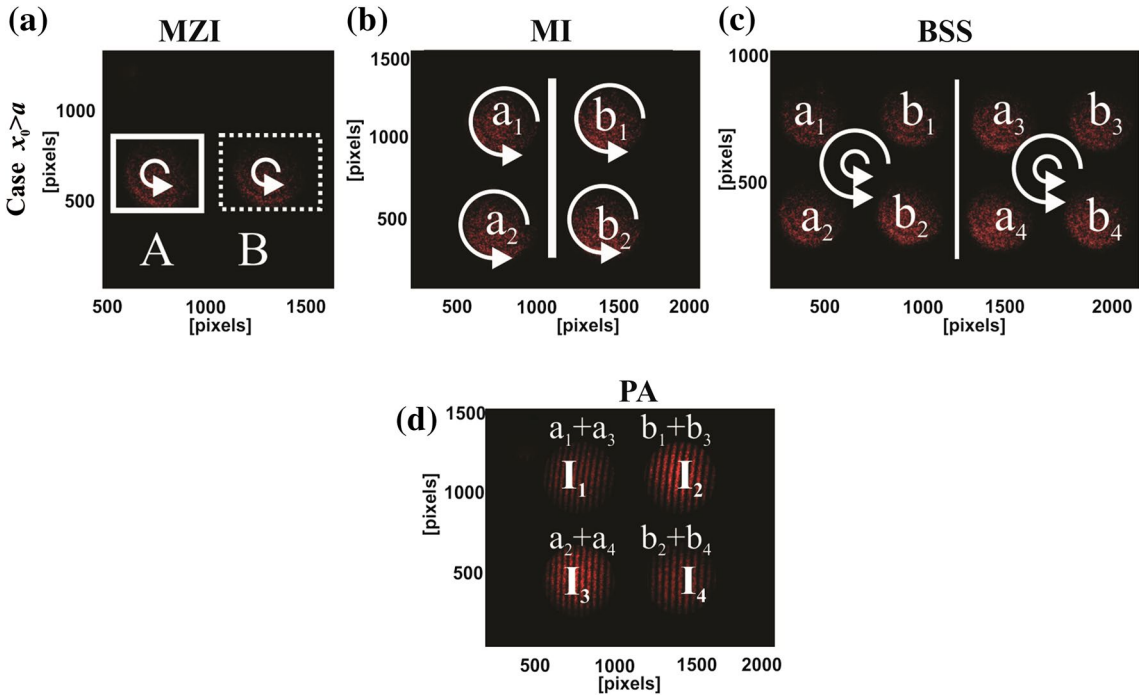

Fig. 2 Case $x_0 > a$. **a** The two beams emerging of the MZI are separated a distance x_0 greater than the beam diameter a. **b** Four beams will be obtained at the output, after passing the Michelson configuration (MI). **c** Eight beams will be obtained at the output, after passing by beam splitter system (BSS). **d** Four interference patterns. a_i,b_i beams replicated. *PA* Polarizer array. I_i interference patterns

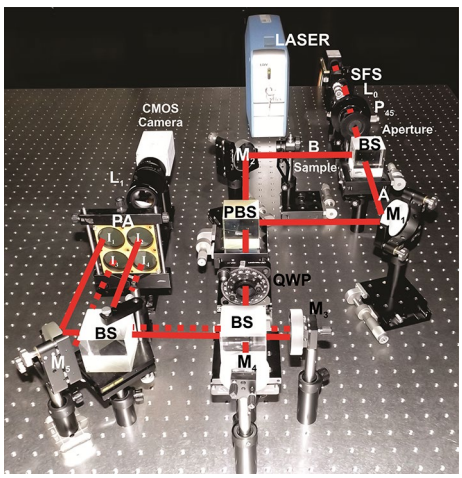

Fig. 3 Picture of the experimental setup. Single-shot Mach–Zehnder Interferometer composed by two replication systems: a Michelson Interferometer configuration and a beam splitter system. Case $x_0 < a$

shifts is limited and the analysis of the polarization states is required to calculate the optical phase.

In the second configuration, the beam separation is smaller than the beam section $x_0 < a$ and the system behaves as a conventional MZI; this is shown in the picture of the setup in Fig. 3. In this case, two beams are interfered in the MZI and the other two remaining systems (MI and BSS) replicate this interference pattern generating four replicas with orthogonal circular polarizations states. In this case, the interferogram replicas are aligned by moving the mirrors M_3–M_5, to adjust the distance x_1. The arrows indicate the polarization states of the base patterns. Figure 4 shows the three stages of the system, as shown in Fig. 1. When $x_0 < a$, a base interferogram is generated at the output of the MZI, as shown in Fig. 4a and it is replicated by the Michelson configuration (MI) (see Fig. 4b), and the beam splitter system (BSS) generating four replicas, and this shown in Fig. 4c. Due to the opposing circular polarizations, it is not possible to see the interferogram at the output on each stage; for viewing purposes, we placed an auxiliary polarizer in each stage and its presented in Fig. 4d to Fig. 4f; after placing the polarizer array (PA) at the corresponding angles (ψ), four interferograms with relative phase shift (ξ) of 90° are generated.

3 Polarization phase-shifting technique

For convenience, taking the case when $x_0 < a$, at the output of the MZI, we obtain the superposition of beams $A + B$, where $A(x,y)$ is the reference beam and $B(x,y)$ is the sample beam (with 45° linear polarization states). Both states will change its polarization properties to circular polarization states in opposite directions after passing through the quarter wave plate

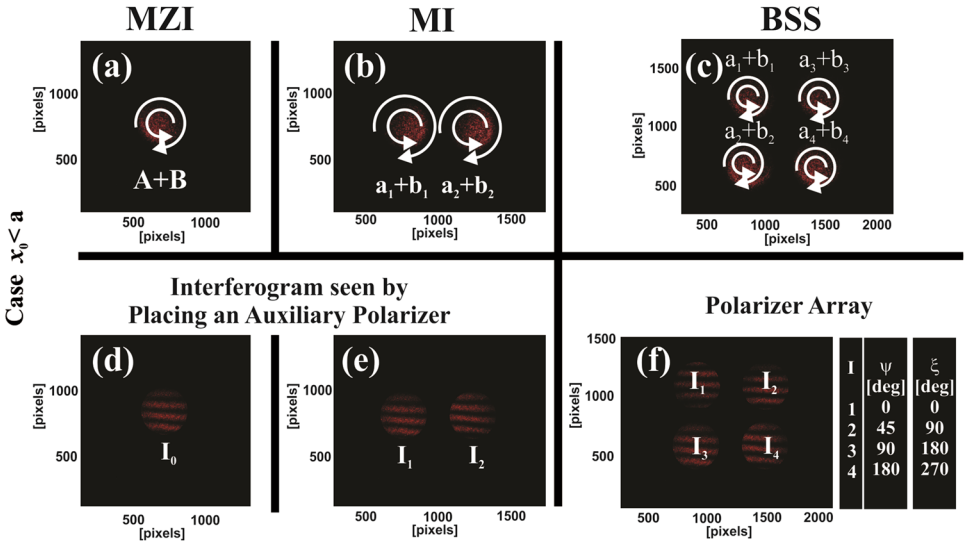

Fig. 4 Case $x_0 < a$. Mach–Zehnder configuration. **a** MZI: pattern with opposing circular polarizations emerging of MZI. **b** Two patterns with opposing circular polarizations emerging of Michelson interferometer (MI) configuration. **c** Four beams after the beam splitter system (BSS). Each replica represents an interference pattern obtained by the MZI. **d** Interference pattern at the output of the MZI. **e** Interference patterns at the output of the MI. **f** Interference patterns at the output of the BSS. a_i,b_i beams replicated. *PA* polarizer array. I_i interference patterns. ξ Phase shifts. ψ Polarizer angles

(QWP). The output beam after the MZI and the QWP can be represented as follows:

$$O(x,y) = \frac{1}{\sqrt{2}}\begin{pmatrix}1\\ i\end{pmatrix}\cdot A(x,y) + \frac{1}{\sqrt{2}}\begin{pmatrix}1\\ -i\end{pmatrix}\cdot B(x,y)\cdot e^{i\phi(x,y)}. \tag{1}$$

After the replication system (MI and BSS) and a linear polarizer at the polarizer array, an interference pattern is obtained as follows:

$$O_\psi(x,y) = P_\psi\cdot\left[\frac{1}{\sqrt{2}}\begin{pmatrix}1\\ i\end{pmatrix}\cdot A(x,y) + \frac{1}{\sqrt{2}}\begin{pmatrix}1\\ -i\end{pmatrix}\cdot B(x,y)\cdot e^{i\phi(x,y)}\right]. \tag{2}$$

After obtaining the complex magnitude of the signal, the interference pattern is obtained and can be depicted as the common interferogram equation with a phase difference $\phi(\boldsymbol{x},\boldsymbol{y})$ between both beams and a controllable phase shift twice the fast axis orientation, $\boldsymbol{\psi}$, of the polarizer as follows:

$$I(x,y) = A^2 + B^2 + AB\cos\left[2\psi - \phi(x,y)\right], \tag{3}$$

where A^2+B^2 corresponds to the bias term and AB is the amplitude modulation. Considering the four patterns generated by the system, each replica obtained will need its polarizer (at the polarizer array) at the following angles: $\psi_1 = 0$; $\psi_2 = \pi/4$; $\psi_3 = \pi/2$; $\psi_4 = 3\pi/4$ with a respective phase shifts (ξ) of 0, $\pi/2$, π, *and* $3\pi/2$.

By the phase replication system and the polarization phase-shifting technique, we were able to generate four simultaneous interference patterns spatially separated in the same image given by the following [29–31]:

$$\begin{aligned} I_1(x,y) &= A^2 + B^2 + AB\cos\left[\phi(x,y)\right]\\ I_2(x,y) &= A^2 + B^2 + AB\sin\left[\phi(x,y)\right]\\ I_3(x,y) &= A^2 + B^2 - AB\cos\left[\phi(x,y)\right]\\ I_4(x,y) &= A^2 + B^2 - AB\sin\left[\phi(x,y)\right], \end{aligned} \tag{4}$$

and the phase at each point is as follows:

$$\phi(x,y) = \tan^{-1}\left[\frac{I_2 - I_4}{I_1 - I_3}\right]. \tag{5}$$

The evaluated phase is wrapped between $[-\pi, \pi]$ due to arctangent function, and to remove the background phase $\phi(x,y)_{\text{ref}}$ [32, 33], we should measure reference phase map beforehand. As a result, the final phase will be the following:

$$\phi(x,y) = \phi(x,y)_{\text{obj}} - \phi(x,y)_{\text{ref}}, \tag{6}$$

where $\phi(x,y)_{\text{ref}}$ is the phase without sample and $\phi(x,y)_{\text{obj}}$ is the phase sample under study. The phase variations are converted to optical path difference (OPD) variations in wavelengths units [λ], using the following equation:

$$\text{OPD} = \frac{\phi(x,y)}{2\pi}\lambda. \tag{7}$$

4 Experimental results and discussions

The optical system uses an He–Ne laser operating at 635 nm and a CMOS camera with a resolution of 2048×1536 pixels (pixel size, 3.2×3.2 μm). Each interferogram was low pass filtered and we employed the Quality-Guided Path Following Method for unwrapping the phase [30–33]. The four polarizers used in the arrangement (PA) are generated by cutting a polarizing sheet with its known transmission axis. The cut of the polarizers is done with a laser cutting machine. For polarized placement at the appropriate angles, a calibrated polarizer is used as an analyzer, and the transmitted intensities are measured. First, it is verified that the four patterns have circular polarizations, by verifying that the intensity does not vary when the analyzer rotates. This guarantees that the correct phase shifts will be obtained when the polarizers

are placed and that the intensity of each pattern will be equal [34–36]. Then, the array of polarizers is placed and we verify that the transmission is zero when the analyzer is orthogonal to the angle of each polarizer, and the transmission is maximum when the analyzer transmission angle is parallel to the angle of each polarizer of the array. To register and process the four interferograms on a single image: first, we place an aperture at the entrance of the system, which is used as reference point, where the four centered interferograms can be found. Then, the program generates a circular mask around each centroid for the four interferograms to separate them. Finally, the optical phase is obtained using the well-known four-step algorithm [34, 37,–37].

Figure 5 shows the intensity variation obtained (without sample) by capturing 100 frames at 10 fps, with a temperature variation interval of $\Delta t \approx 0.2$ °C. Figure 5a shows the four-phase shifted interferograms obtained in a single shot; the average in time obtained for each pixel (interferogram enclosed at a circle) is shown in Fig. 5b; the corresponding standard deviation is shown in Fig. 5c. Figure 5d shows the intensity variation of the representative pixel enclosed in the dotted rectangle (pixel coordinate: 1380, 550) of the marked interferogram at Fig. 5a. The average intensity obtained corresponds to 6.14 with a standard deviation of 3.04 in a 256 Gy level depth range capture. This result shows that the intensity variations are stable to environmental noise [37]. Figure 6a shows the interferograms generated without sample (reference) and Fig. 6b shows the resulting OPD.

The experimental samples used are shown in Fig. 7. Figure 7a shows the acetate sheet on which a deformation has been made by pressing it at the center. The acetate sheet is homogeneous and has low birefringence. However, because the sample could induce errors in the polarization states, and therefore, in the phase shifts, small adjustments were made in the polarizer angles of the polarizer array (PA) to obtain phase shifts of $\pi/2$ [34, 35]. The variations in contrast were corrected by normalizing the patterns and performing a spatial filtering [35–38]. Figure 7b shows the way in which the acetate was stressed to generate a dynamic variation in the optical phase. Figure 7c shows the flame used to generate temperature variations that can be measured by the system. Although the flame varies with time, the optical phase can be recovered for a specific instant of time, because the system captures instantaneously the four interferograms. In Fig. 7d, the pseudoscorpion sample is shown, from which the legs of the ventral region are analyzed. This sample is fixed on a slide holder. Blood cells are not shown by their scale; these were deposited by 'smear' on a microscope slide.

Figure 8a shows the four patterns generated when a deformation on an acetate sheet is induced and the resulting OPD calculated from the optical phase map in shown in Fig. 8b. Because the mean-refractive index of the sample is

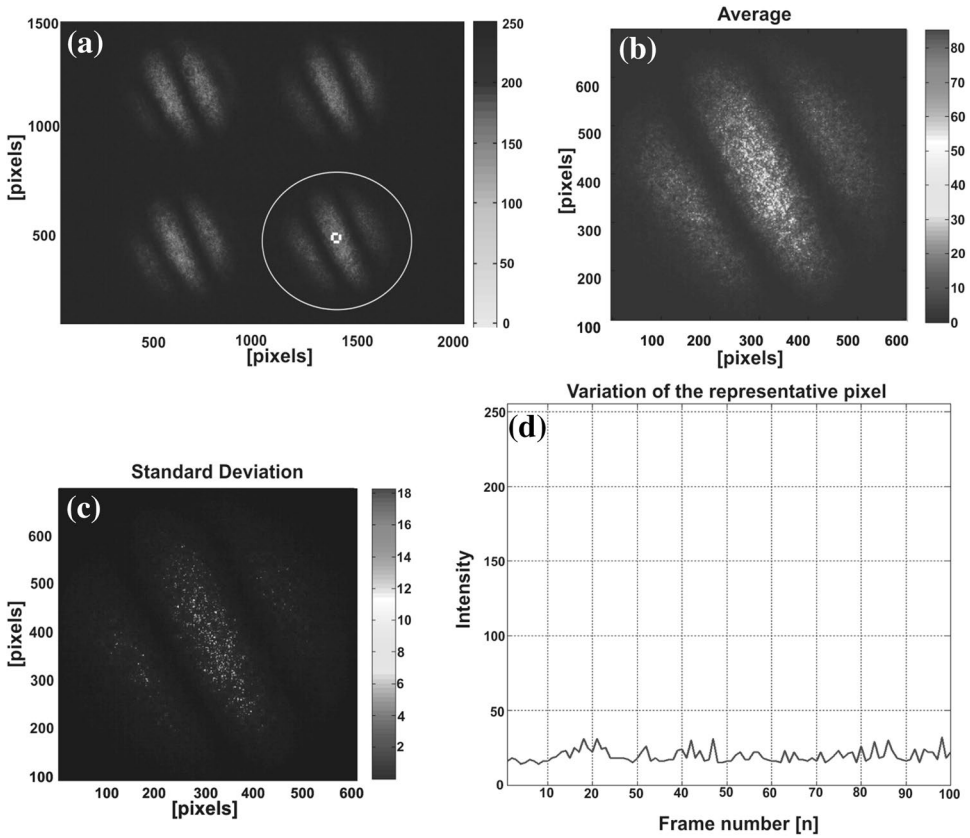

Fig. 5 **a** Intensity variation of representative interferogram. **b** Average obtained. **c** Standard deviation by each pixel. **d** One-pixel variation. Average ≈ 6.14. Standard deviation≈ 3.04

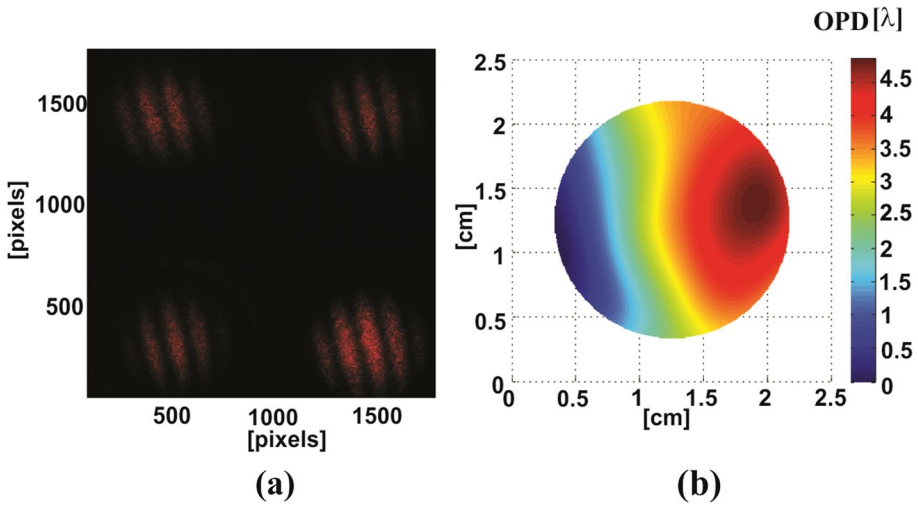

Fig. 6 Reference wavefront. **a** Four simultaneous interference patterns. **b** OPD

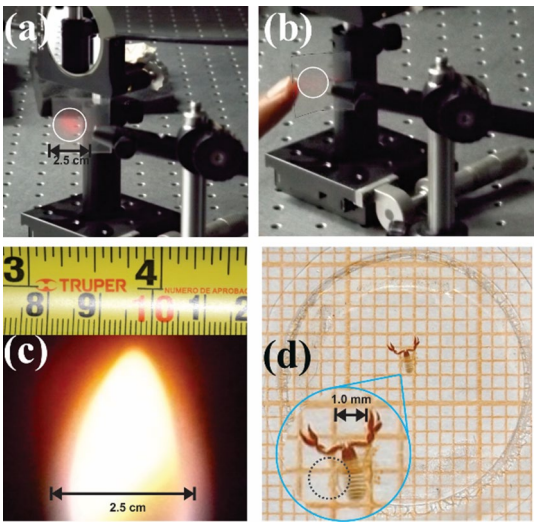

Fig. 7 Experimental samples. **a** Acetate sheet. **b** Deformation generated on acetate sheet. **c** Flame of a bunsen burner. **d** Pseudoscorpion

$\Delta n = 1.485$, we can calculate the mean thickness ≈ 12.20 µm. To demonstrate the advantages of the proposed system, Fig. 9 shows a dynamic phase object corresponding to a deformation of an acetate sheet under tension. Representative frame is presented. The acetate has been fixed on the mechanical components, and it has been bent by tensing it. Video 1 shows the dynamic variation that is generated when the acetate sheet is restored to its resting position.

We employed acetate as a sample due of the knowledge of its parameters and availability on the lab. In addition, as we are employing polarization properties on the interferometric system, we also added compensation techniques due of the birefringence presented. In the experiments, errors in the polarization are corrected using the theory developed in Ref. [34, 35]. To verify the polarization properties of the acetate sample, the intensities were measured before and after placing the sample. The difference between the phase

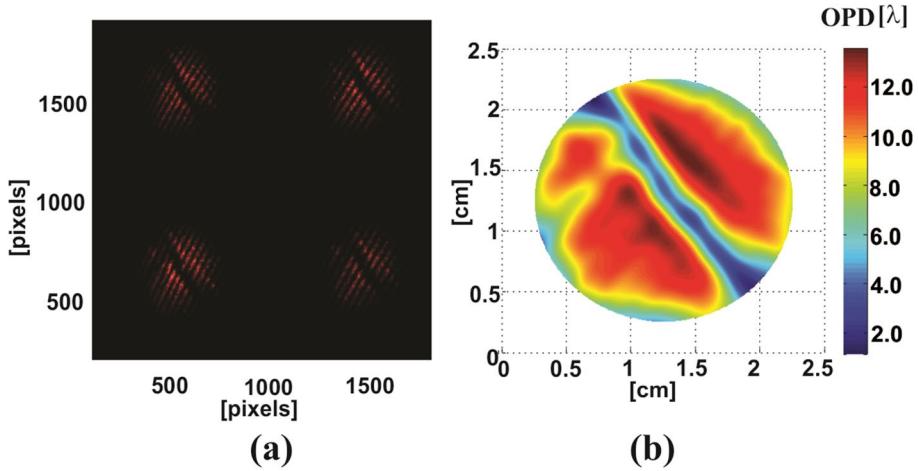

Fig. 8 Acetate sample. **a** Four simultaneous interference patterns. **b** OPD

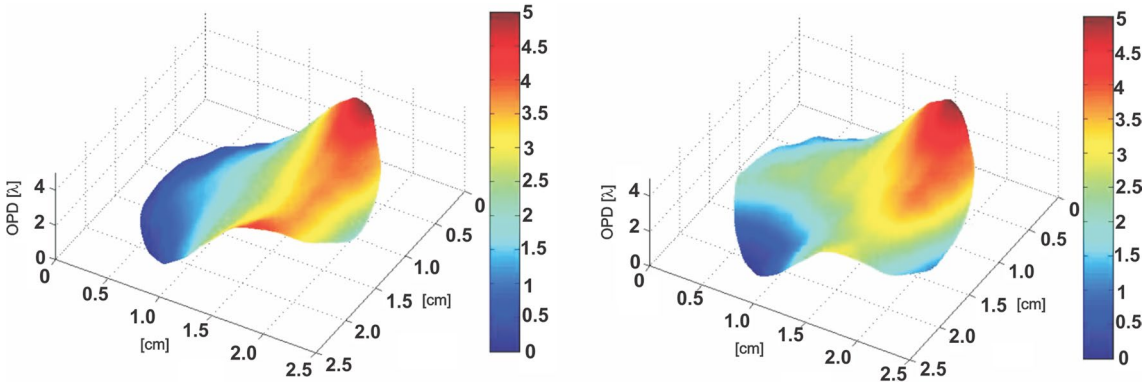

Fig. 9 Dynamic phase object. Deformation of the surface of an acetate sheet under tension. Representative frames (Video 1)

shifts was calculated [35], and for the particular case of this sample, these are negligible.

Figure 10 shows the phase change generated by the air flow that crosses the trajectory of beam A generated by the flame of a Bunsen burner; in Fig. 10a, the simultaneous interferograms are shown, and in Fig. 10b, the OPD is associated with the phase change.

For the results shown in Figs. 11 and 12, a microscope system has been added a microscope objective (MO) with magnification of 60× and lens of 200 mm of focal length, on each arm of the MZI. This is done to be able to analyze microscopic samples, such as red blood cells and the legs of the pseudoscorpion. Figure 11 shows the experimental results for the pseudoscorpion legs, the sample was fixed with a resin called glycerinated gelatin which is used to fix organic samples to microscope's slides.

The interesting part of the study corresponds to the legs of the ventral region, since this is one way of partially identifying the order of the species [24]. Figure 11a shows the four interferograms obtained in instantaneous capture of the camera. Figure 11b and c shows the Optical Path Difference (OPD) of the sample. Figure 12 shows the (OPD) induced by a group of Red Blood Cells (RBC); their morphology is obtained as a very important parameter in the biomedical field to diagnose diseases. Figure 12a shows the four interferograms captured in one shot of the camera and Fig. 12b and c presents the OPD for all RBC under study. Figure 12d shows the OPD obtained for the RBC enclosed in the rectangle shown in Fig. 12c; it can be noticed that the OPD, and it allows us to calculate the mean thickness, which is calculated as $\mathrm{OPD}/\Delta n = 3.2\ \mu\mathrm{m}$, where Δn mean value of the RBC refraction index, was, assumed 1.395 for the RBC [24].

In addition, to retrieve phase variation in time, the implemented system has capabilities for obtaining spiral patterns. This is achieved by placing a telescopic system on each arm of the MZI to generate two radially sheared beams and a phase allocation on one of the arms of the MZI configuration. The spiral patterns were obtained, when achieving approximately a π/2 phase shift by introducing a tilted transparent plate in the path of the spherical wavefront of one MZI's arm, obstructing half of the wavefront. This method can be used as an alternative technique to obtain spiral patterns without using Bessel beams or using an axicon, for

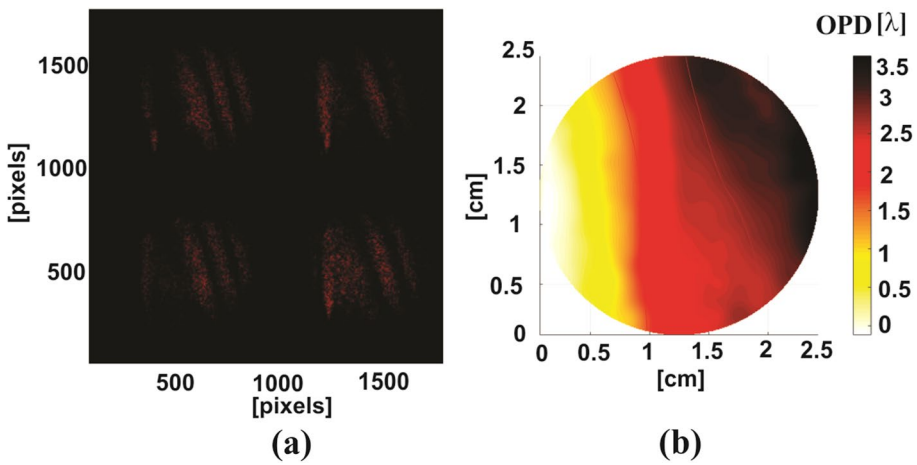

Fig. 10 **a** Four simultaneous interference patterns. **b** OPD

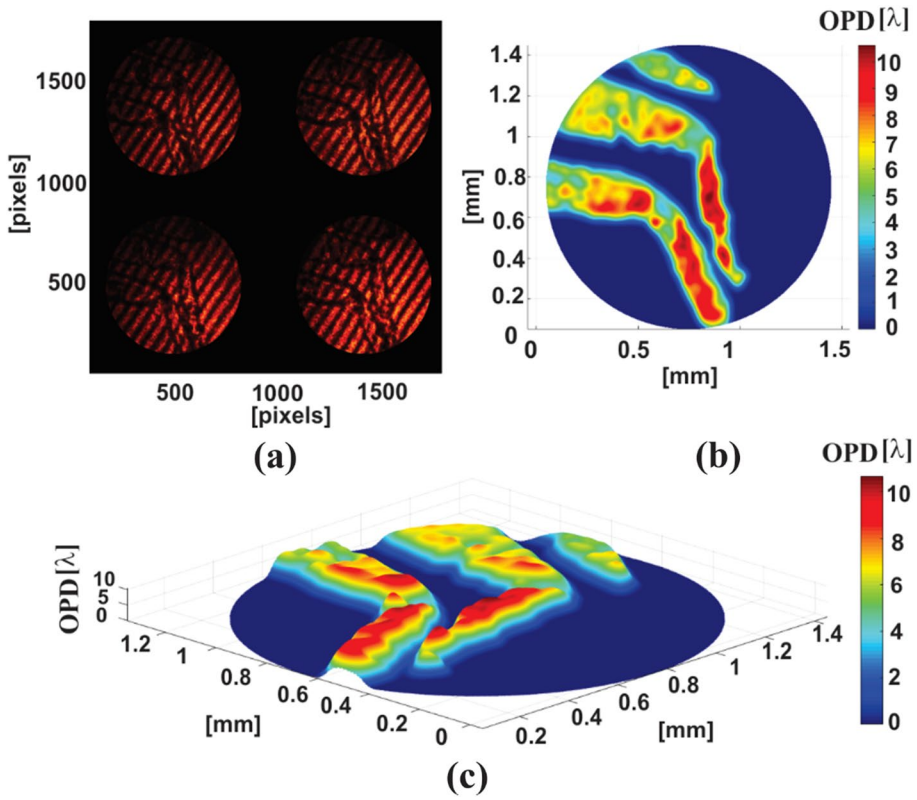

Fig. 11 Pseudoscorpion legs. **a** Four simultaneous interference patterns. **b, c** OPD

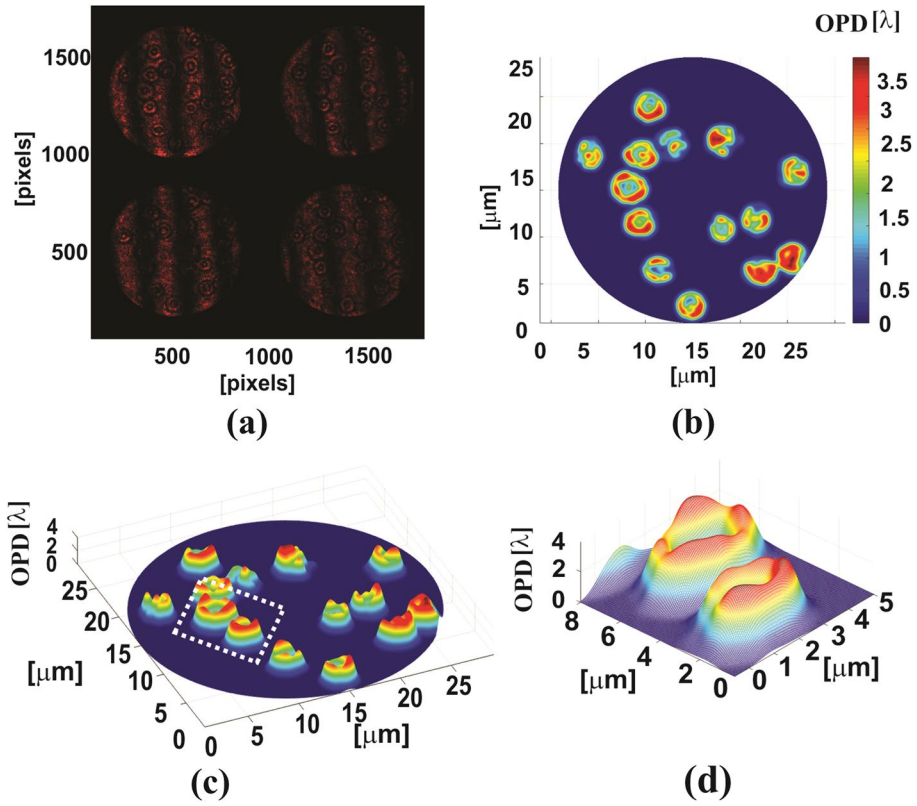

Fig. 12 Red blood cells. **a** Four simultaneous interference patterns. **b, c** OPD. **d** OPD of two RBC

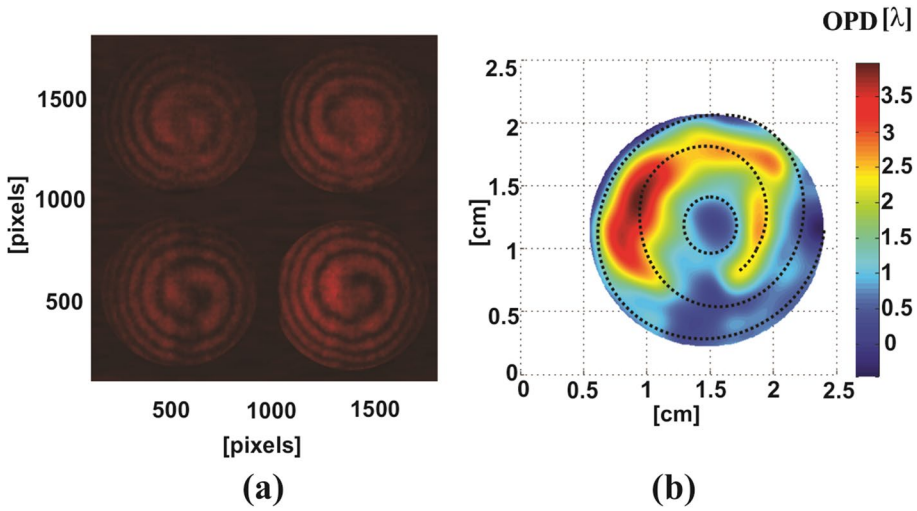

Fig. 13 Spiral interferometry. **a** Four simultaneous patterns. **b** OPD

example, because the inclined obstruction generates a dislocation like that appearing in a spiral-phase plate [38].

Figure 13a shows a four simultaneous spiral patterns and Fig. 13b shows the phase obtained; we can see that the phase has a phase vortex in the center (enclosed at doted circle) as predicted by the theory; this preliminary result obtained through experimentation with the described setup, which allowed us to obtain interferograms with spiral symmetry [38–40].

5 Conclusions

We reported a simultaneous phase-shifting technique based in a Mach–Zehnder interferometer (MZI) and two replicating systems integrated by a Michelson interferometer and cube beam splitter. The complete implementation can generate four interference patterns with independent phase shifts. This configuration is capable to analyze phase variation in time, and can be adapted for the conventional and microscopic measurements. The proposal is based on the replication of the output phase obtained by a Mach–Zehnder configuration. The interferogram replication system is composed by Michelson configurations and a beam splitter, which, aligned in such case, allows us to retrieve four interferograms obtained from the Mach–Zehnder interferometer. The interferogram registration is done by employing an aperture at the entrance of the system to identify a common point on the image captured by the camera. Under our working conditions, we did not require any numerical compensation; we are not employing a micropolarizing array or diffractive elements to retrieve the necessary interferometric replicas to achieve the measurements, or robust algorithms for alignment the pixelated mask to the cameras. The experimental results show a simple method to generate spiral beams, which are useful for the determination of the sign of the phase. In addition, this configuration can be used also as a shear interferometer by placing the sample at the entrance of the MZI and this will be considered for future implementations.

Acknowledgements The authors would like to thank the anonymous reviewers for their valuable comments and suggestions to improve the quality of the paper. Author N. I. Toto-Arellano acknowledges the support provided by the National Council of Science and Technology (CONACYT) by the project A1-S-20925. A. Montes Pérez acknowledges the support provided by the Vice-Rectoría de Investigation y Estudios de Posgrado (VIEP) for project MOPA-EXC17-G and the Programa para el Desarrollo Profesional Docente (PRODEP) under project DSA/ 103.5 / 15/7449. Author V.H. Flores-Muñoz acknowledges Programa para el Desarrollo Profesional Docente (PRODEP) for the grant provided (UPBIC-PTC-022).

References

1. Carré, P.: Installation et utilisation du comparateurphotoélectrique es interferétiel du Bureau International des Poids et Measures. Bureau International des Poids et Measures **2**, 13–23 (1966)
2. Crane, R.: Interference phase measurement. Appl. Opt. 8, 538 (1969)
3. Bruning, J.H., Herriott, D.R., Gallagher, J.E., Rosenfeld, D.P., White, A.D., Brangaccio, D.J.: Digital wavefront measuring interferometer for testing optical surfaces and lenses. Appl. Opt. **13**, 2693 (1974)
4. Bruning, J.H.: Fringe Scanning Interferometers. In: Malacara, D. (ed.) Optical Shop Testing, Wiley, New York, (1978)
5. Hardy, J., Feinleib, J., Wyant, J.C.: Real time phase correction of optical imaging systems. OSA Topical Meeting on Opt. Propagation through Turbulence, Boulder (1974)
6. Wyant, J.C.: Use of an ac heterodyne lateral shear interferometer with real-time wavefront correction systems. Appl. Opt. **14**, 2622 (1975)
7. Malacara, D.: Optical Shop Testing, 3rd edn. Wiley, New York (2007)
8. Hariharan, P.: Basics of Interferometry. Elsevier, Amsterdam (2007)

9. Lasyk, L., Lukomski, M., Bratasz, L.: Simple digital speckle pattern interferometer (DSPI) for investigation of art objects. Opt. Appl. **41**(3), 687–700 (2011)
10. Morris, M.N., Millerd, J., Brock, N., Hayes, J., Saif, B.: Dynamic phase-shifting electronic speckle pattern interferometer. Proc. SPIE **5869**, 58691B-1 (2005)
11. Toto-Arellano, N.I., Serrano-García, D.I., Martínez-García, A., Rodríguez Zurita, G., Montes-Pérez, A.: 4D profile of phase objects through the use of a simultaneous phase shifting quasi-common path interferometer. J. Opt. **13**(11), 115502 (2011)
12. Millerd, J.E., Brock, N., Hayes, J., North-Morris, M., Novak, M., Wyant, J.: Pixelated phase-mask dynamic interferometer. Proc. SPIE **5531**, 304–314 (2004)
13. Kothiyal, M.P., Delisle, C.: Rotating analyzer heterodyne interferometer: error sources. Appl. Opt. **24**, 2288–2290 (1985)
14. Okoomian, H.J.: A two-beam polarization technique to measure optical phase. Appl. Opt. **8**(11), 2363–2365 (1969)
15. Junwei Min, B., Yao, P., Gao, R., Guo, J., Zheng, Ye, T.: Parallel phase-shifting interferometry based on michelson-like architecture. Appl. Opt. **49**, 6612–6616 (2010)
16. Abdelsalam, D.G., Yao, B., Gao, P., Min, J., Guo, R.: Single-shot parallel four-step phase shifting using on-axis Fizeau interferometry. Appl. Opt. **51**, 4891–4895 (2012)
17. Toto-Arellano, N.I., Serrano-García, D.I., Martínez-García, A.: Parallel two-step phase shifting interferometry using a double cyclic shear interferometer. Opt. Express **21**, 31983–31989 (2013)
18. Awatsuji, Y., Sasada, M., Kubota, T.: Parallel quasi-phase-shifting digital holography. Appl. Phys. Lett. **85**, 1069–1071 (2004)
19. Awatsuji, Y., Tahara, T., Kaneko, A., Koyama, T., Nishio, K., Ura, S., Kubota, T., Matoba, O.: Parallel two-step phase-shifting digital holography. Appl. Opt. **47**, D183–D189 (2008)
20. Toto-Arellano, N.I., Serrano-Garcia, D.I., Rodriguez-Zurita, G.: Optical path difference measurements with a two-step parallel phase shifting interferometer based on a modified Michelson configuration. Opt. Eng. **56**(9), 094107 (2017)
21. Barrientos-García, B., Moore, A.J., Pérez-López, C., Wang, L., Tschudi, T.: Transient deformation measurement with electronic speckle pattern interferometry by use of a holographic optical element for spatial phase stepping. Appl. Opt. **38**(28), 5944–5947 (1999)
22. Barrientos-García, B., Moore, A.J., Pérez-López, C., Wang, L., Tschudi, T.: Spatial phase-stepped interferometry using a holographic optical element. Opt. Eng. **38**(12), 2069–2074 (1999)
23. Wyant, J.C.: Dynamic interferometry. Opt. Photon. News **14**(4), 36–41 (2003)
24. Toto-Arellano, N.I.: 4D measurements of biological and synthetic structures using a dynamic interferometer. J. Mod. Opt. **64**(sup. 4), S20–S29 (2017)
25. Koliopoulos, C.L.: Simultaneous phase-shift interferometer. Proceeding of SPIE 1531, Advanced Optical Manufacturing and Testing II (1992)
26. Shock, I., Barbul, A., Girshovitz, P., Nevo, U., Korenstein, R., Shakeda, N.T.: Optical phase nanoscopy in red blood cells using low-coherence spectroscopy. J. Biomed. Opt. **17**(10), 101509 (2012)
27. Pham, H., Ding, H., Sobh, N., Do, M., Patel, S., Popescu, G.: Off-axis quantitative phase imaging processing using CUDA: toward real-time applications. Biomed. Opt. Express **2**(7), 1781–1793 (2011)
28. Flores, M.V.H., Toto Arellano, N.-I., Serrano García, D.I., Martínez García, A., Rodríguez Zurita, G., García Lechuga, L.: Measurement of mean thickness of transparent samples using simultaneous phase shifting interferometry with four interferograms. Appl. Opt. **55**, 4047–4051 (2016)
29. Malacara, D., Servin, M., Malacara, Z.: Phase Detection Algorithms in Interferomgram Analysis for Optical Testing. Wiley, New York (2005)
30. Ghiglia, C., Pritt, M.D.: Chapter.4 in "Two-Dimensional Phase Unwrapping: Theory, Algorithms, and Software". Wiley, New York (1998)
31. Servin, M., Estrada, J.C., Quiroga, J.A.: The general theory of phase shifting algorithms. Opt. Express **17**, 21867–21881 (2009)
32. Kerr, D., Kaufmann, G.H., Galizzi, G.E.: Unwrapping of interferometric phase-fringe maps by the discrete cosine transform. Appl. Opt. **35**(5), 810–816 (1996)
33. Ghiglia, D.C., Romero, L.A.: Robust two-dimensional weighted and unweighted phase unwrapping that uses fast transforms and iterative methods. JOSA A **11**(1), 107–117 (1994)
34. Rodriguez-Zurita, G., Meneses-Fabian, C., Toto-Arellano, N.I., Vázquez-Castillo, J.F., Robledo-Sánchez, C.: One-shot phase-shifting phase-grating interferometry with modulation of polarization: case of four interferograms. Opt. Express **16**, 7806–7817 (2008)
35. Toto-Arellano, N.I., Rodriguez-Zurita, G., Meneses-Fabian, C., Vazquez-Castillo, J.F.: Phase shifts in the Fourier spectra of phase gratings and phase grids: an application for one-shot phase-shifting interferometry. Opt. Express **16**, 19330–19341 (2008)
36. Serrano-Garcia, D.I., Toto-Arellano, N.-I., Parra-Escamilla, G.A., Martínez García, A., Rodríguez-Zurita, G., Otani, Y.: Multiwavelength wavefront detection based on a lateral shear interferometer and polarization phase-shifting techniques. Appl. Opt. **57**, 6860–6865 (2018)
37. Toto-Arellano, N.I., Serrano-García, D.I., Rodríguez-Zurita, G., Pérez, A.M., Parra-Escamilla, G.: Temporal measurements of transparent samples with four simultaneous interferograms by using a Mach–Zehnder Interferometer. Opt. Commun. **429**, 80–87 (2018)
38. Rodríguez-Zurita, G., Toto-Arellano, N.I., Arroyo-Carrasco, M.L., Meneses-Fabían, C., Castillo, J.F.V.: Experimental observation of spiral patterns by obstruction of Bessel beams: application of single shot phase-shifting interferometry. Conf. on Lasers and Electro-Optics/Pacific Rim 2009 (Optical Society of America), 2009, ThE1 4 (2009)
39. Galushko, Y., Mokhun, I.: Detection of the vortices signs in the scalar fields. Opt. Appl. **38**(4), 705–713 (2008)
40. Anguiano-Morales, M., Salas-Peimbert, D.P., Trujillo-Schiaffino, G., Hernandez, D., Toto-Arellano, N.I.: Bessel beam spatially truncated. Opt. Commun. **284**(6), 1504–1509 (2006)